Am J Transl Res 2026;18(4):2882-2895
www.ajtr.org /ISSN:1943-8141/AJTR0168424

Original Article

FBXO31-induced ABL2 ubiquitination increases cystine-glutamate antiporter-mediated ferroptosis and inhibits malignant progression in triple-negative breast cancer

Yuhao Zhang[1*], Jingjing Luo[1*], Qing Xu[1], Xianzhen Zeng[1], Xinyu Wang[1,5], Hui Xu[2], Xueshan Pan[1,3], Tong Cao[4], Hua Huang[3*], Jia Ma[1,3*]

[1]Bengbu Medical University Key Laboratory of Cancer Research and Clinical Laboratory Diagnosis, Bengbu Medical University, Bengbu 233030, Anhui, China; [2]Department of Laboratory Medicine, School of Laboratory Medicine, Bengbu Medical University, Bengbu 233030, Anhui, China; [3]Department of Biochemistry and Molecular Biology, School of Laboratory Medicine, Bengbu Medical University, Bengbu 233030, Anhui, China; [4]Department of Clinical Laboratory, The First Affiliated Hospital of Bengbu Medical University, Bengbu 233004, Anhui, China; [5]Anhui Provincial Key Laboratory of Tumor Evolution and Intelligent Diagnosis and Treatment, Bengbu Medical University, Bengbu 233030, Anhui, China. [*]Equal contributors.

Received August 28, 2025; Accepted February 25, 2026; Epub April 15, 2026; Published April 30, 2026

Abstract: F-box only protein 31 (FBXO31) has been implicated in tumorigenesis and development across various human cancers. However, the role of FBXO31 in breast cancer progression remains poorly understood. In this study, we identified FBXO31 as a tumor suppressor in triple-negative breast cancer (TNBC), where it inhibited cell proliferation, migration, and invasion. Furthermore, FBXO31 promoted cystine-glutamate antiporter (xCT)-mediated ferroptosis in TNBC cells. Notably, overexpression of FBXO31 suppressed tumor growth in mice. Mechanistically, ABL-related gene (ABL2) was identified as a novel ubiquitin substrate of FBXO31. FBXO31 specifically interacted with ABL2 and promoted ABL2 ubiquitination and subsequent degradation through its F-box motif. Functionally, ABL2 acted as an oncogenic factor in TNBC cells by promoting cell proliferation, migration, and invasion, while inhibiting xCT-mediated ferroptosis. Rescue experiments showed that FBXO31 inhibited TNBC progression at least partly through downregulating ABL2 expression. Collectively, our findings reveal a novel molecular mechanism for TNBC progression and provide a potential therapeutic strategy for its treatment.

Keywords: FBXO31, ABL2, ubiquitination, ferroptosis, triple negative breast cancer

Introduction

Breast cancer (BC) ranks first in incidence and second in cancer-related mortality worldwide [1, 2]. Triple-negative breast cancer (TNBC), characterized by lost expression of the estrogen receptor (ER), progesterone receptor (PR), and human epidermal growth factor receptor 2 (Her-2), represents the most aggressive subtype of BC with the poorest prognosis [3, 4]. Owing to the absence of these related receptor targets, patients with TNBC do not benefit from established endocrine or targeted drugs [5]. Thus, the standard treatment for nonsurgical TNBC continues to be cytotoxic chemotherapy [5]. In the past few years, immunotherapy has been demonstrated to be a promising approach to improving TNBC outcomes [4, 6]. Even so, compared with those of non-TNBC subtypes, TNBC still exhibits higher recurrence and mortality rates and remains the most challenging subtype of BC [5].

Ubiquitin modification, a critical regulatory machinery of protein stability and function, regulates cell biological processes, several of which are associated with diverse human diseases [7]. E3 ubiquitin ligases (E3 ligases) are the crucial components of the ubiquitination cascade because they are endowed with substrate specificity and directly bind to the substrates [7]. Recent studies have shown that

https://doi.org/10.62347/ZKXJ6492

F-box E3 ligases, as constituent units of SKP1-CUL1-F-box (SCF) E3 ligase complex, play key roles in cancer progression [8, 9]. FBXO31, a member of F-box E3 ligases, has been suggested to mediate tumorigenesis and cancer progression in various human tumors [10-13]. In BC, however, the role of FBXO31 in tumor biology remains unclear and controversial. It has been reported that FBXO31 can inhibit cell proliferation and arrest the cell cycle, functioning as a tumor suppressor in BC [14, 15]. However, another study has shown that FBXO31 is overexpressed in BC samples and may serve as an independent poor prognostic factor for BC [16]. Thus, the function and molecular mechanisms of FBXO31 in BC require further elucidation.

ABL2, also named ARG (ABL-related gene), is a member of the Abelson (ABL) family of tyrosine kinases [17]. Mutant ABL kinases were initially identified as drivers of human leukemia, such as BCR-ABL1 [17]. ABL tyrosine kinases regulate signaling pathways involved in cell survival, growth, migration, and invasion [18, 19]. ABL kinases, including ABL2, have been proven to promote tumor progression and metastasis in several human solid tumors [18-20]. For example, enhanced ABL2 expression and ABL2 amplification have been detected in BC and are associated with worse prognosis [21]. Furthermore, ABL2 has also been reported to promote EMT (Epithelial-Mesenchymal Transition) and metastasis cascade in BC [22]. However, contradictory roles for ABL2 in tumor growth have been observed between *in vivo* and *in vitro* results, which may depend on cellular context in BC [21].

Here, we report a novel underlying molecular mechanism of FBXO31-mediated ABL2 ubiquitination and degradation in BC. In particular, we found that FBXO31 and its downstream target ABL2 play a pivotal role in ferroptosis, a newly emerged form of iron-dependent oxidative cell death. Our findings may provide a novel therapeutic strategy for patients with BC.

Materials and methods

Reagents and antibodies

The following reagents were used in this study: CCK-8 kit (Cell Counting Kit-8) (Beyotime Biotechnology), Lipo8000 (Beyotime Biotechnology), ROS (Reactive Oxygen Species) detection kit (Biotech Biotechnology Co., Ltd.), ferrous ion detection kit (Elabscience), and MDA (Malondialdehyde) detection kit (Nanjing Jiancheng Bioengineering Institute). Antibodies included: FBXO31 Polyclonal antibody (27294-1-AP, Proteintech), ABL2 Polyclonal antibody (17693-1-AP, Proteintech), cystine-glutamate antiporter (xCT) antibody (DF12509, Affinity), glutathione peroxidase 4 (GPX4) antibody (DF6701, Affinity), Anti-beta Actin Rabbit pAb (GB11001-100, Servicebio), and DYKDDDDK tag Polyclonal antibody (Flag tag epitope) (20543-1-AP, Proteintech).

Cell culture

Human Triple-negative breast cancer (TNBC) cell lines were obtained from the Cell Bank of the Chinese Academy of Sciences. BT549 cells were cultured in RPMI 1640 medium (Gibco), and MDA-MB-231 cells were maintained in DMEM medium (Gibco). Both media were supplemented with 10% FBS (Fetal Bovine Serum) (Gibco) and 1% penicillin-streptomycin (Biosharp). Cells were incubated at 37°C with 5% CO_2. FBXO31 and ABL2 overexpression plasmids were purchased from Youbio (Hunan, China).

CCK-8 assay for cellular activity

Depending on the cell type, 3500 to 5500 cells were seeded per well in a 96-well plate with 200 μL medium. Each group included five sub-wells, and PBS (Phosphate-Buffered Saline) was added to the outermost wells to prevent evaporation. On the following day, complete medium was added to adjust the total volume to 100 μL per well, and cells were incubated for 24, 48, and 72 h. Absorbance was determined by an enzyme-linked immunosorbent assay (ELISA) reader (Bio-Rad) at 450 nm, and the IC_{50} and IC_{75} values were calculated.

Transfection of siRNAs (small interfering RNAs) and plasmids

Fbxo31 and ABL2 cDNAs were cloned into pcDNA3.1 by Youbio (Hunan, China), and siRNAs were synthesized by Hanbio Tech (Shanghai, China). The siRNA sequences used in this study are provided in **Table 1**. The above constructs and siRNAs were transfected into BT549 and MDA-MB-231 cells using Lipo8000 transfection reagent (Beyotime Biotechnology),

Table 1. The siRNA sequences

Target Gene	siRNA Number	Sequence (5'-3')
FBXO31	siRNA-FBXO31#1	GCCTGGAGATTGTGATGCT
FBXO31	siRNA-FBXO31#2	GATGACCCTATGAGATTCA
ABL2	siRNA-ABL2#1	CCTCGTCATCTGTTGTTCCAT
ABL2	siRNA-ABL2#2	CGGTCAGTATGGAGAGGTTTA

Table 2. Primer sequences for target genes

Target Gene	Primer Type	Sequence (5'-3')
FBXO31	Forward primer	GTACGACAACTGCCTGACC
FBXO31	Reverse primer	AGGCTTGATGAGGTCGTCG
ABL2	Forward primer	CTGGGTGCCAAGCAACTACA
ABL2	Reverse primer	TACACACGTCCCTCGTACCT

followed by western blot analysis to confirm gene overexpression and knockdown efficiency.

qRT-PCR (quantitative real-time polymerase chain reaction)

Total RNA was extracted and reverse transcribed using the TAKARA kit (item number RR036A). Using the qRT-PCR kit from Vazyme, cDNA synthesized by reverse transcription was added to the premix, and qRT-PCR was performed on anABI7500. The primer sequences for FBXO31 and ABL2 are detailed in **Table 2**.

Western blotting

Cells were lysed with RIPA (Radio Immunoprecipitation Assay buffer) buffer containing PMSF (Phenylmethylsulfonyl Fluoride), and protein concentration was quantified using a BCA (Bicinchoninic Acid) protein quantification kit at 560 nm. Proteins were denatured by heating at 100°C for 5 minutes in a metal bath. Proteins were fractionated on a 10% sodium dodecyl sulfate-polyacrylamide gel and subsequently transferred onto activated PVDF (Polyvinylidene Fluoride) membranes. The membrane strip was placed in a diluted antibody solution and incubated at 4°C overnight. On the subsequent day, membranes were washed three times with TBST (Tris-Buffered Saline with Tween-20) buffer. The secondary antibody was meticulously applied and incubated for 1 to 2 hours. Once the unbound secondary antibody had been thoroughly washed away, the protein bands were made visible using a chemiluminescence detection system.

Lipid ROS measurement

After treatment, cells in six-well plates were carefully washed with PBS. Subsequently, 1 mL basal medium was added to each well. Next, 0.5 μL DCFH-DA (2',7'-Dichlorodihydrofluorescein Diacetate) was added to each well (except blank wells). The plate was gently shaken to mix and incubated for 30 minutes. After incubation, cells were washed with PBS and digested with trypsin. The cell suspension was transferred into centrifuge tubes and centrifuged at 1500 r/min for 5 minutes. The supernatant was discarded, and cells were washed twice with 1 mL PBS by resuspension and centrifugation at 1500 r/min for 5 minutes. This washing procedure was performed twice to thoroughly remove any residual impurities. Following the last centrifugation, the supernatant was discarded, and the cells were resuspended in 300 μL PBS. The resuspended cell sample was maintained on ice until analysis by a flow cytometer. A Beckman flow cytometer was used for detection. Since the fluorescence spectrum of DCF is very similar to that of FITC, the detection of DCF was carried out according to the parameter settings of FITC. After the detection was completed, the relevant data were collected and analyzed.

Fe^{2+} assay

Reagents were prepared strictly following the ferrous ion assay kit instructions and equilibrated to room temperature before use. For the cells in a 6-cm dish, the old medium was discarded. The cells were washed once with PBS. Subsequently, 1 mL PBS was added. A cell scraper was used to collect the cells into 1.5-mL EP tubes, and the cells were gently pipetted to mix. Cell numbers were counted and recorded accurately. After counting, the suspension was centrifuged at 300 gravitational units (g) for 10 minutes, and the supernatant was discarded. Based on the cell count, 200 μL of reagent I was added per 1×10^6 cells. The solution was mixed well and then lysed on ice for 10 minutes. Subsequently, the lysate was centrifuged at 15,000 g for 10 minutes, and the supernatant was saved for further use. Reagents were added step-by-step in accordance with the directions of the ferrous ion detection kit, and the results were calculated according to the provided formula.

MDA assay

Reagents were prepared according to the Malondialdehyde (MDA) Assay Kit instructions and equilibrated to room temperature. Cells cultured in 6-cm dish had their medium discarded and were washed once with PBS before adding 1 mL PBS. Cells were scraped into 5-mL EP tubes and disrupted on ice using a cell crusher set to 200-300 W. The cells were crushed for 5 seconds, followed by a 15-second interval. This cycle was repeated 3-5 times. The entire cell-crushing process was carried out on ice. After thoroughly mixing the disrupted cell suspension, 1 μL was pipetted for protein concentration measurement. Reagents were added step-by-step as per the kit instructions. The centrifuge tube was sealed with its lid, and a small hole was made in it. The tube was vortexed to mix the contents well. Subsequently, it was positioned in a water bath maintained at 95°C for 40 minutes. After heating, the tube was immediately removed and cooled in ice. The cooled sample was centrifuged at 4000 r/min for 10 minutes. The supernatant was carefully collected. A microplate reader was used to measure the OD value of each tube at a wavelength of 532 nm. Ultimately, the calculations were performed according to the formula provided in the kit instructions.

Immunoprecipitation

For immunoprecipitation analysis, cells were lysed using cold NP-40 (Nonidet P-40) lysis buffer supplemented with a protease inhibitor cocktail sourced from Thermo Fisher Scientific. The cell lysates were incubated with magnetic beads conjugated to either HA or Flag-tag antibodies (manufactured by Sino Biological, China). This incubation step was carried out to enable the specific attachment of the target proteins to the beads. After the incubation period, the magnetic beads were washed three times with TBST buffer. This washing step was crucial to remove any non-specific interactions that might have occurred between the beads and other components in the cell lysate. Upon completion of washing, the proteins bound to the beads were subsequently eluted by boiling in SDS loading buffer, a method that effectively disrupts the bonds holding the proteins to the beads.

In vivo ubiquitination assay

To detect *in vivo* ubiquitination of ABL2, cells were co-transfected with Myc-tagged ubiquitin and the specified plasmids. After 36 hours, cells were treated with 10 μM of MG132 (Sigma) for 6 hours. After the incubation period, the cells were gathered together and lysed in NP-40 lysis buffer, enabling the extraction of cellular components for further analysis. Lysates were incubated with HA-tag magnetic beads. Subsequently, the beads were meticulously washed three times with TBST. After that, the bound proteins were eluted by immersing the beads in boiling SDS loading buffer. Finally, the pulled-down proteins underwent analysis by western blotting to detect the target proteins.

Protein stability analysis

The cycloheximide (CHX) chase assay was performed to evaluate protein stability and calculate the half-life of the specific target protein. Cells were transfected with the indicated constructs and incubated for 48 hours to ensure robust protein expression. After the transfection was completed, cells were treated with cycloheximide at a concentration of 20 μg/mL (Sigma) to suppress the *de novo* synthesis of proteins. At specified time points after cycloheximide treatment, cells were harvested and lysed to extract proteins. Protein abundances were quantified by western blotting using specific antibodies against the protein of interest. Band intensities were analyzed by densitometry, and the protein half-life was calculated by plotting the relative protein levels over time.

Animal experimentation

Stably FBXO31-overexpressing MDA-MB-231 cells were generated, and 4-week-old BALB/c Nude mice were purchased. After one week of acclimatization, each mouse was injected with approximately 1×10^6 cells in the axilla. One week after the completion of tumor seeding, tumor volume was recorded every three days for 15 consecutive days. Once the last recording was done, mice were sacrificed following ethical guidelines. Tumors were then surgically removed from the mice. After that, the excised tumors were promptly weighed, and their weights were recorded. Finally, the tumors were photographed from multiple angles to capture comprehensive visual data about their characteristics. The tissues were ground, and tissue proteins were extracted. Gene expression was analyzed by western blotting, and a part of the tumor tissues was retained for Hematoxylin and Eosin (H&E) staining. All BALB/c Nude mice used in the experiment were raised in an Specific Pathogen Free (SPF) - grade barrier environment and euthanized immediately after the experiment.

Statistical analysis

Data are presented as mean value accompanied by the standard deviation (SD). To assess the statistical significance, both the t-test and one-way analysis of variance (ANOVA) statistical methods were used. A *p*-value less than 0.05 was considered significant (*P < 0.05; **P < 0.01; ***P < 0.001; ****P < 0.0001).

Results

FBXO31 expression decreases in breast cancer (BC)

Using TIMER 2.0 (http://timer.cistrome.org/), we downloaded a unified, standardized pan-cancer dataset from The Cancer Genome Atlas (TCGA) database and found that FBXO31 expression was significantly reduced in most tumors, especially in BC (Figure S1A). Next, we accessed the GEPIA website (http://gepia.cancer-pku.cn/) and obtained a BC dataset from TCGA, which confirmed that FBXO31 expression was significantly lower in tumor tissues than in adjacent normal tissues (Figure S1B). Using the UALCAN online database (https://ualcan.path.uab.edu), we further analyzed FBXO31 expression in BC across different clinical parameters. FBXO31 expression was lower in BC, particularly in the Luminal and Triple-negative breast cancer (TNBC) subtypes (Figure S1C, S1D), and decreased progressively with increasing tumor stage (stages 1-4) (Figure S1E). Finally, survival analysis from the Kaplan-Meier Plotter database (https://kmplot.com/) demonstrated that high FBXO31 expression was associated with better survival in patients with BC compared to low expression (Figure S1F). Clinical IHC (Immunohistochemistry) validation [15] confirms significant downregulation of FBXO31 protein in breast cancer tissues compared to normal adjacent tissues, consistent with our bioinformatic findings and supporting its tumor-suppressive role in breast cancer.

Overexpression of FBXO31 inhibits cell proliferation, migration, and invasion in Triple-negative breast cancer (TNBC) cells

CCK-8 assays were conducted to assess cell proliferation. The results showed that FBXO31 overexpression significantly inhibited cell proliferation in TNBC cell lines, including BT549 and MDA-MB-231 cells (**Figure 1A**). Conversely, transfection with FBXO31 siRNA markedly promoted cell proliferation compared to the control group (**Figure 1B**). Additionally, we performed Transwell assays on TNBC cells transfected with FBXO31 cDNA or siRNA. Overexpression of FBXO31 significantly suppressed cell migration and invasion (**Figure 1C**), whereas knockdown of FBXO31 by siRNA notably enhanced both migration and invasion abilities of the cells (**Figure 1D**).

FBXO31 promotes cystine-glutamate antiporter (xCT)-mediated ferroptosis in TNBC cells

FBXO31 overexpression plasmid and siRNA were separately transfected into BT549 and MDA-MB-231 cells. To analyze the impact of FBXO31 on ferroptosis, we detected several key ferroptosis regulators, including Ferroptosis Suppressor Protein 1 (FSP1), Acyl-CoA Synthetase Long-Chain Family Member 4 (ACSL4), GPX4, and xCT. Western blot analysis indicated that elevated FBXO31 expression reduced the levels of ferroptosis suppressors GPX4 and xCT (**Figure 2A**). Conversely, FBXO31 knockdown by siRNA increased their expression (**Figure 2B**). However, FBXO31 overexpression did not significantly affect the protein levels of FSP1 or ACSL4 (Figure S2). Consistent with the inhibitory roles of GPX4 and xCT in ferroptosis, FBXO31 overexpression increased ROS (Reactive Oxygen Species) (**Figure 2C**), Fe^{2+} (**Figure 2E**), and MDA (Malondialdehyde) (**Figure 2F**) levels in TNBC cells. The results for FBXO31 siRNA treatment showed decreased levels of ROS, Fe^{2+}, and MDA (**Figure 2D**, **2G**, **2H**). We performed Co-IP (Co-Immunoprecipitation) assays in BT549 TNBC cells to determine whether FBXO31, as an E3 ubiquitin

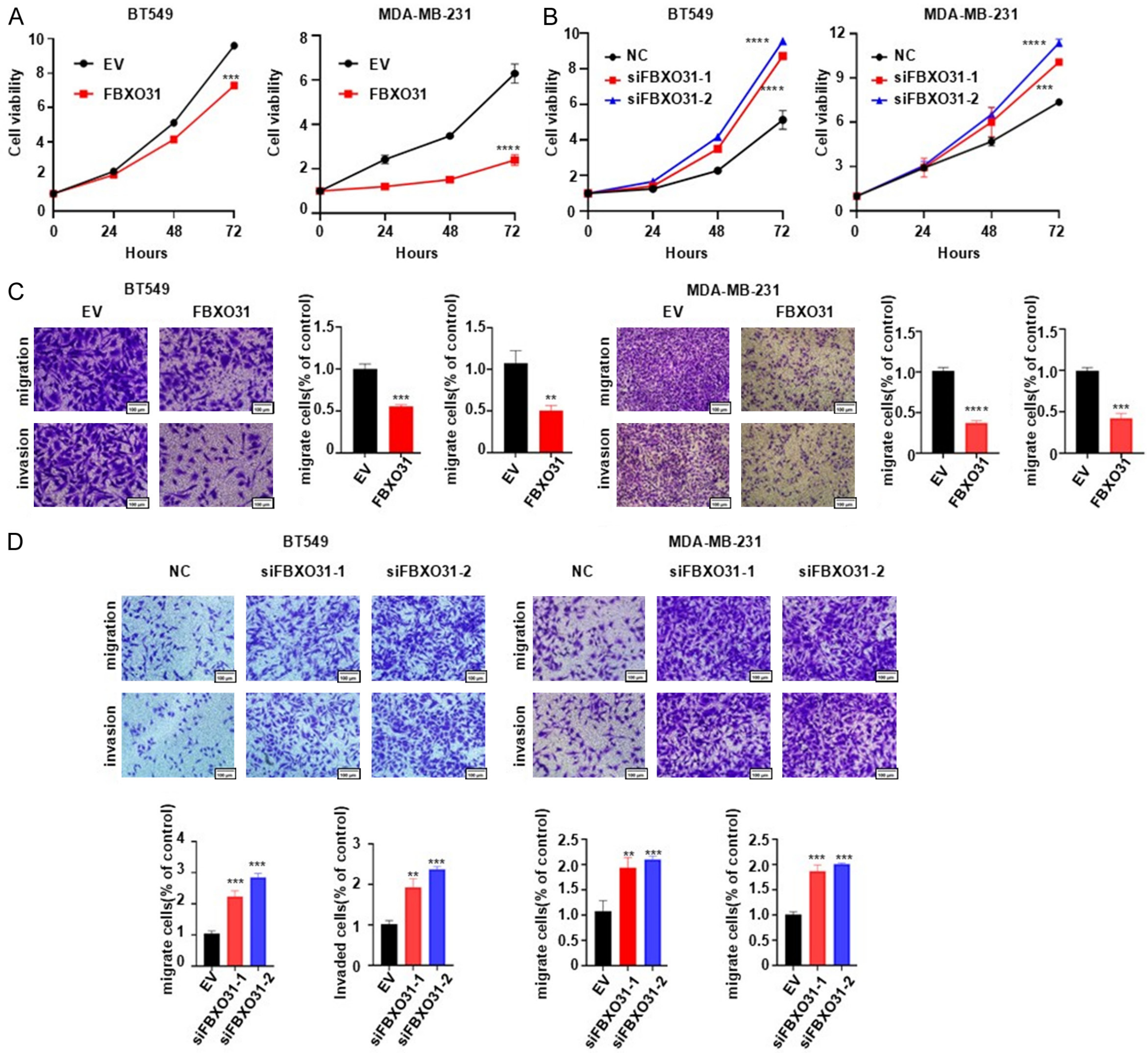

Figure 1. (A, B) CCK-8 assays to detect cell growth of BT549 and MDA-MB-231 cells transfected with indicated FBXO31 cDNA (A) or FBXO31 siRNA (B). (C, D) Transwell assays to analyze cell migration and invasion capacity of BT549 and MDA-MB-231 cells transfected with FBXO31 cDNA (C) or FBXO31 siRNA (D). ** indicates P < 0.01, *** indicates P < 0.001, **** indicates P < 0.0001.

ligase, directly interacts with GPX4 or xCT, which it regulates. However, when co-expressed, an HA antibody against xCT or GPX4 did not co-precipitate Flag-tagged FBXO31. These results suggest that FBXO31 regulates the xCT/GPX4 ferroptosis pathway through an indirect mechanism.

FBXO31 promotes ABL2 ubiquitination and subsequent degradation through its F-box motif

As illustrated in our previous study, LC-MS/MS (Liquid Chromatography-Tandem Mass Spectrometry) was performed to identify targets of FBXO31 [10]. Additionally, the peptide sequence of ABL2 was detected in the mass spectrometry results (**Figure 3A**). Western blot analysis further revealed that FBXO31 overexpression markedly decreased ABL2 protein levels, whereas FBXO31 knockdown elevated them (**Figure 3B** and **3C**). Notably, ABL2 mRNA levels remained barely unchanged in FBXO31-overexpression cells (**Figure 3D**), while the half-life of ABL2 protein was markedly decreased (**Figure 3E** and **3F**). Moreover, co-immunoprecipitation (Co-IP) and ubiquitination assays demonstrated that FBXO31 bound to ABL2 and subsequently promoted its ubiquitination (**Figure 3G**, **3H**). Collectively, these data sug-

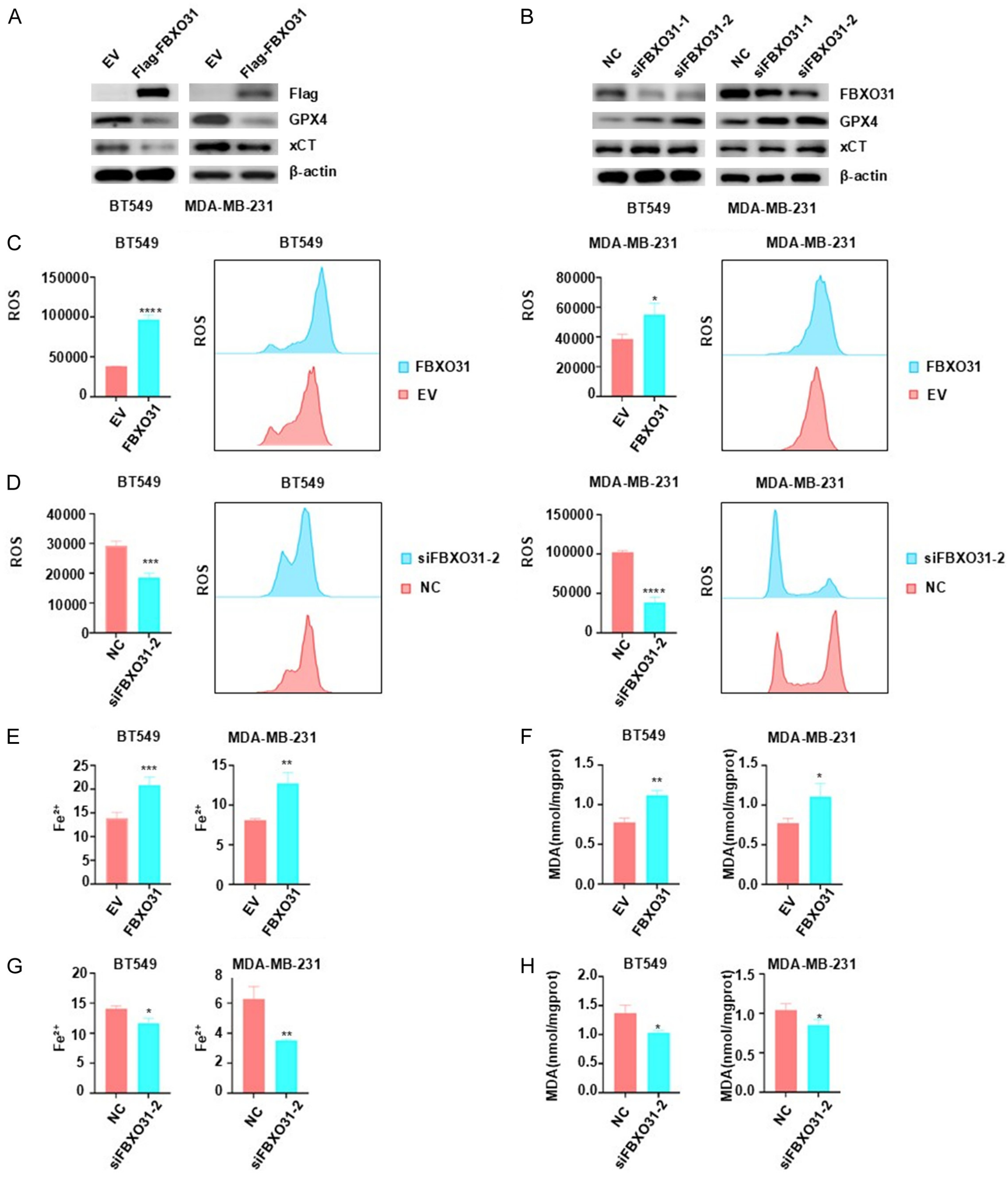

Figure 2. (A, B) BT549 and MDA-MB-231 cells were transfected with FBXO31 cDNA or FBXO31 siRNA, respectively, and western blot was performed to examine changes in Glutathione Peroxidase 4 (GPX4) and cystine-glutamate antiporter (xCT) expression. (C, E, F) BT549 and MDA-MB-231 cells were transfected with FBXO31 cDNA to detect cellular ROS (Reactive Oxygen Species) levels (C), Fe^{2+} levels (E), and MDA (Malondialdehyde) levels (F). (D, G, H) BT549 and MDA-MB-231 cells were transfected with FBXO31 siRNA to detect cellular ROS levels (D), Fe^{2+} levels (G), and MDA levels (H). * indicates $P < 0.05$, ** indicates $P < 0.01$, *** indicates $P < 0.001$, **** indicates $P < 0.0001$.

gest that FBXO31-mediated ABL2 degradation occurred in a ubiquitination-dependent manner. Previous studies have shown that FBXO31's F-box (F-box domain-deleted FBXO31) domain facilitates substrate ubiquitination and degradation but is not involved in substrate binding. Consistently, our Co-IP results showed that FBXO31 ΔF-box bound to ABL2 as efficient-

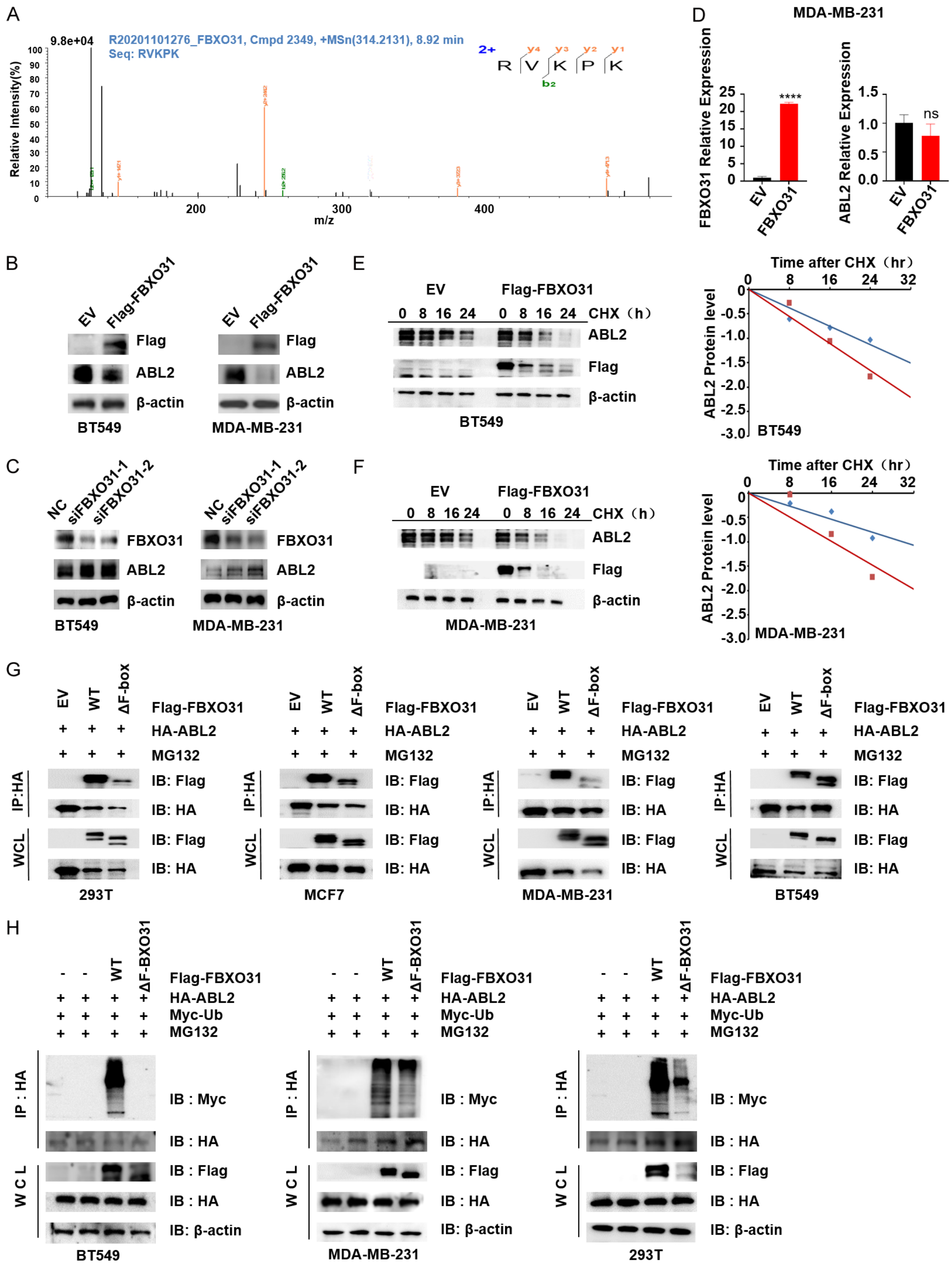

Figure 3. (A) LC-MS/MS (Liquid Chromatography-Tandem Mass Spectrometry) was performed to screen for targets of FBXO31, and the peptide sequence of ABL2 was detected in the mass spectrometry results. (B, C) Western blot results showed FBXO31 overexpression markedly decreased ABL2 protein levels (B), whereas its knockdown elevated them (C). ABL2 mRNA levels were barely changed in FBXO31-overexpression cells (D). (E, F) Detection of the half-life of ABL2 protein in Triple-negative breast cancer (TNBC) cells (BT549, MDA-MB-231) transfected with FBXO31 cDNA. (G, H) Co-IP (Co-Immunoprecipitation) (G) and ubiquitination (H) assays demonstrated that FBXO31 could bind to ABL2 and subsequently elevate ABL2 ubiquitination levels. **** indicates P < 0.0001, ns indicates P > 0.05.

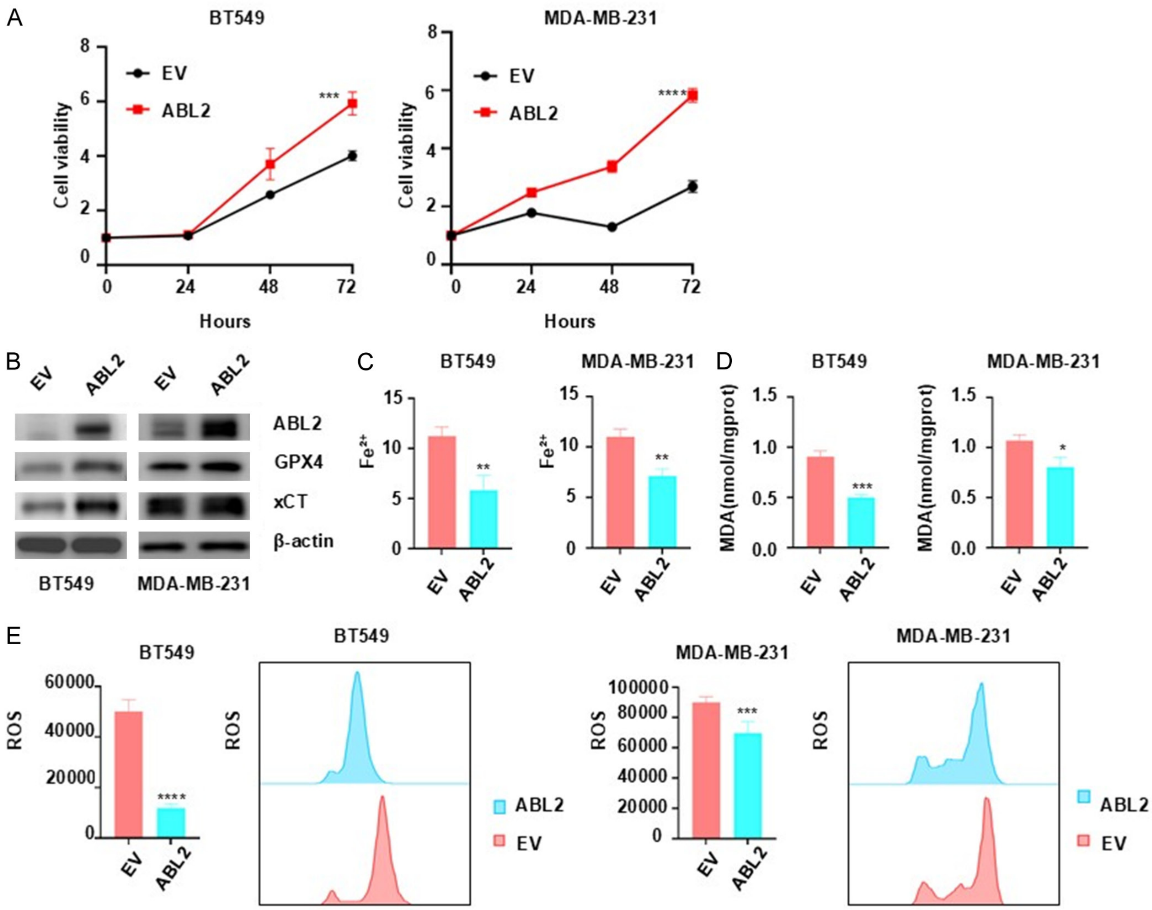

Figure 4. (A) CCK-8 assays to detect cell growth of BT549 and MDA-MB-231 cells transfected with ABL2 cDNA. (B) BT549 and MDA-MB-231 cells were transfected with ABL2 cDNA, and western blot was performed to examine changes in GPX4 and xCT expression. (C-E) BT549 and MDA-MB-231 cells were transfected with ABL2 cDNA to detect cellular Fe^{2+} levels (C), MDA levels (D) and ROS levels (E). * indicates $P < 0.05$, ** indicates $P < 0.01$, *** indicates $P < 0.001$, **** indicates $P < 0.0001$.

ly as wild-type FBXO31 (**Figure 3G**). Moreover, ubiquitination assays demonstrated that FBXO31 ΔF-box weakened ABL2 ubiquitination compared to the wild-type FBXO31 (**Figure 3H**).

ABL2 expression increases in BC samples

We analyzed ABL2 expression using multiple online tools with transcriptome data from TCGA. TIMER 2.0 analysis revealed that ABL2 expression was significantly elevated in most tumor types, particularly in BC (Figure S3A). Data from the UALCAN database confirmed higher ABL2 expression in BC tumors, especially in Luminal and TNBC subtypes (Figure S3B, S3C). Moreover, ABL2 expression increased with advancing tumor stage (stages 1-3) in patients with BC (Figure S3D). Kaplan-Meier analysis demonstrated that patients with high ABL2 expression had significantly poorer survival outcomes compared to those with low expression (Figure S3E).

ABL2 promotes cell proliferation while inhibiting ferroptosis in TNBC cells

Functional assays were performed to investigate the oncogenic role of ABL2 in TNBC. CCK-8 assays showed that transfection with ABL2 cDNA significantly enhanced the proliferation of TNBC cell lines BT549 and MDA-MB-231 (**Figure 4A**). Conversely, ABL2 knockdown by siRNA markedly reduced cell proliferation in BT549 and MDA-MB-231 cells (Figure S4A). Additionally, GPX4 and xCT expression levels increased following ABL2 overexpression (**Figure 4B**) but decreased after ABL2 knockdown (Figure S4B). Measurement of ferroptosis

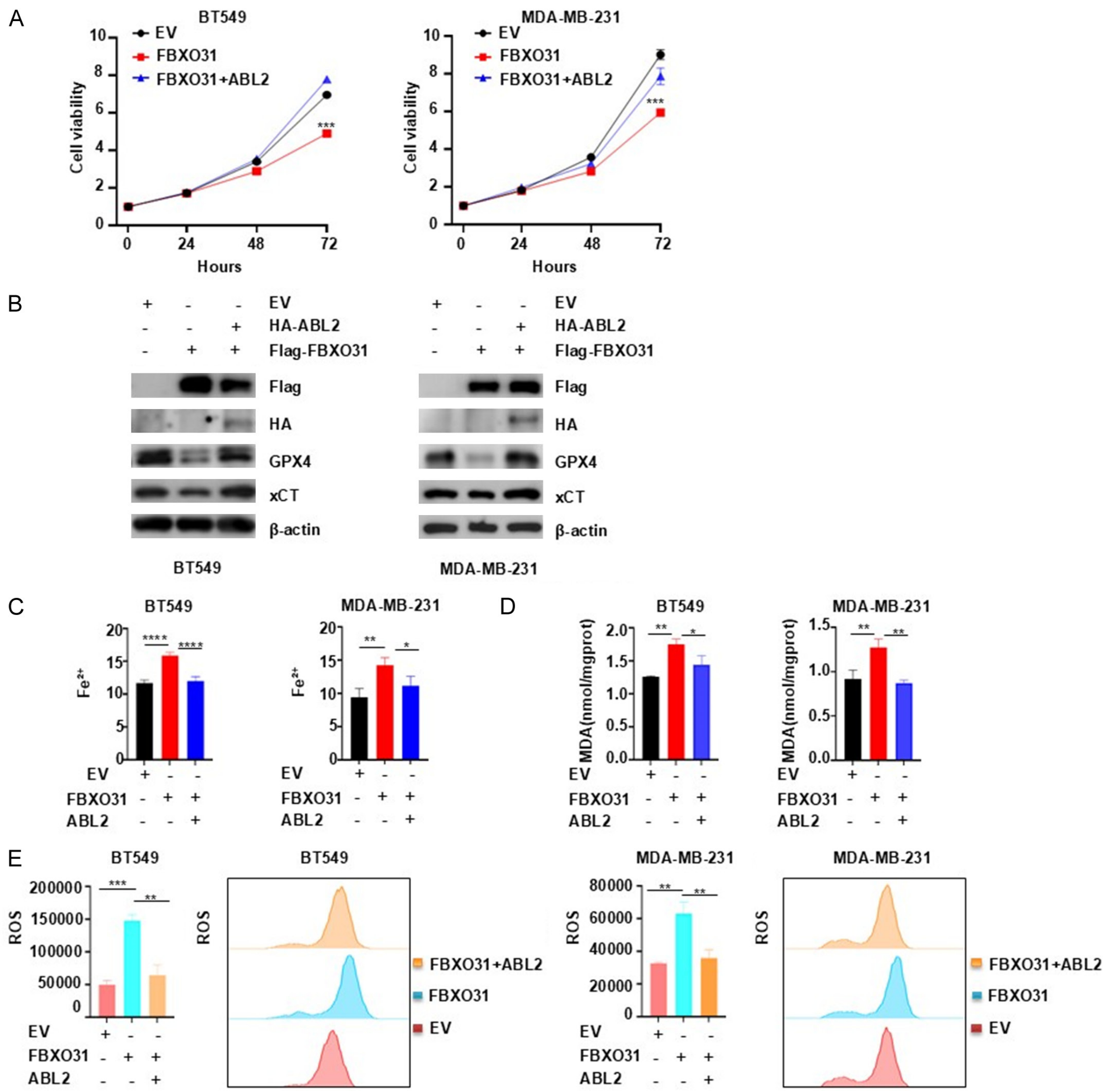

Figure 5. (A) CCK-8 assays for the effect of simultaneous overexpression of FBXO31 and ABL2 on cell growth. (B) Simultaneous transfection of FBXO31 and ABL2 cDNA in TNBC cells and detection of changes in GPX4, xCT protein expression by western blotting. (C-E) Detection of Fe^{2+} (C), MDA (D), ROS (E) levels in co-transfected cells. * indicates $P < 0.05$, ** indicates $P < 0.01$, *** indicates $P < 0.001$, **** indicates $P < 0.0001$.

markers showed that ABL2 overexpression reduced levels of ROS, Fe^{2+}, and MDA (**Figure 4C-E**), while ABL2 knockdown increased these parameters (Figure S4C-E).

Rescue experiments show that FBXO31 inhibits cancer progression partly by down-regulating ABL2 expression in TNBC

To determine whether FBXO31 exerts its tumor suppressive effects through ABL2 down-regulation, rescue experiments were performed by simultaneous overexpression of FBXO31 and ABL2 on cell proliferation and ferroptosis. As shown in **Figure 5A**, ABL2 overexpression reversed the growth inhibition effects induced by FBXO31 overexpression in TNBC cells. Western blot analysis confirmed that ABL2 overexpression reversed the FBXO31-mediated ABL2 down-regulation (**Figure 5B**). Consistently, ABL2 re-expression attenuated FBXO31-mediated suppression of GPX4 and xCT expression (**Figure 5B**). Moreover, ROS, Fe^{2+}, and MDA measurements revealed that FBXO31 increased their levels, which were reversed by additional ABL2 up-regulation

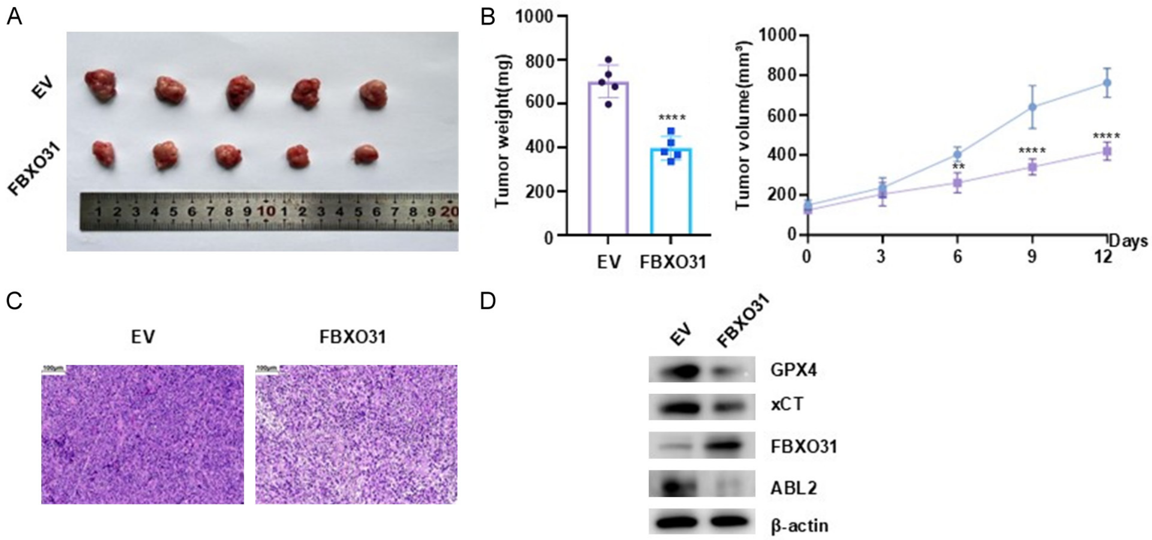

Figure 6. (A) Pictures of tumor mass dissected from FBXO31-overexpressing xenograft mouse models. (B) Tumor weights and tumor volumes of dissected tumor mass in (A). (C) Resected tumor tissues were analyzed by H&E staining. (D) Western blotting was performed on proteins extracted from dissected tumor mass. ** indicates $P < 0.01$, **** indicates $P < 0.0001$.

(**Figure 5C-E**). These results suggest that FBXO31 inhibits cell proliferation and induces ferroptosis partially by targeting ABL2.

FBXO31 inhibits tumor growth in mice

BALB/c Nude mice were divided into two groups (five mice per group) and inoculated in the axilla with MDA-MB-231 cells stably transfected with either an empty vector group (EV) or FBXO31. Tumors from the FBXO31-overexpressing mice showed significantly reduced weight and volume compared to controls (**Figure 6A** and **6B**). Resected tumor tissues were analyzed by H&E staining and western blotting (**Figure 6C** and **6D**). Western blot analysis demonstrated high FBXO31 expression accompanied by decreased levels of ABL2, xCT, and GPX4 in FBXO31-overexpressing tumors (**Figure 6D**). These findings indicate that FBXO31 inhibits tumor growth by down-regulating ABL2 expression.

Discussion

Triple-negative breast cancer (TNBC) is the most malignant subtype of breast cancer (BC), accounting for approximately 15% to 20% of all patients with BC [6]. Thus, understanding the complex molecular mechanisms and identifying novel therapeutic targets for TNBC are urgently needed. In the present study, we identified a novel FBXO31-ABL2 signaling axis that regulates TNBC progression and ferroptosis, providing new targets for TNBC treatment.

Previous studies, including ours, have demonstrated that FBXO31 plays either pro-tumorigenic or anti-tumorigenic roles in various human cancers [10-13, 23]. However, the function of FBXO31 in BC remains controversial and needs to be further explored. In our current study, we found that FBXO31 enhanced cell ferroptosis while suppressing cell proliferation and motility in TNBC cells. Furthermore, overexpression of FBXO31 inhibited xenograft tumor growth *in vivo.* Bioinformatic analysis based on TCGA data revealed that FBXO31 mRNA expression was lower in BC compared to normal tissues, and FBXO31 up-regulation was correlated with better survival in BC. Thus, our findings demonstrate that FBXO31 functions as a tumor suppressor in TNBC.

Ferroptosis is a recently characterized form of iron-dependent cell death, marked by lethal accumulation of lipid peroxidation on cellular membranes [24]. Evidence suggests that ferroptosis acts as an antitumor mechanism by inhibiting tumor growth, enhancing immunotherapy efficacy, and overcoming resistance to conventional cancer therapies [25-27]. The susceptibility of cells to ferroptosis depends on the balance between ferroptosis drivers, such as polyunsaturated fatty acid-phospholipid (PUFA-PL) synthesis, lipid peroxidation, and iron toxicity, and defense mechanisms, including GPX4-dependent and independent systems [24, 25]. GPX4 is a key enzyme involved in neutralizing lipid peroxides and protecting against ferroptosis, relying on the uptake of extracellular cystine mediated by xCT [24, 25]. FBXO31 has been suggested to promote ferroptosis by ubiquitinating GPX4 in cholangiocarcinoma cells [13]. Consistently, our study showed that FBXO31 promoted ferroptosis in TNBC cells by down-regulating xCT and GPX4 expression, indicating that FBXO31 enhanced ferroptosis through the xCT/GPX4 pathway.

Although FBXO31 functions as an E3 ubiquitin ligase, our Co-IP assays revealed no direct interaction with xCT and GPX4 in TNBC cell lines. While previous work confirmed that FBXO31 directly binds GPX4 in cholangiocarcinoma [13], this interaction may not occur in TNBC due to its distinct tumor microenvironment, cofactor availability, and post-translational modification profiles. Moreover, E3 ligases often regulate downstream targets indirectly-by modulating upstream signaling pathways or transcriptional machinery. Thus, we propose that FBXO31 may regulate GPX4 and xCT indirectly, possibly through intermediary molecules.

As an E3 ubiquitin ligase, FBXO31 is responsible for substrate recognition and ubiquitination, subsequently leading to proteasome-directed degradation [29]. Previous studies have demonstrated that FBXO31 targets several oncogenic substrates, including cyclinD1, DUSP6, MDM2, and OGT, thereby functioning as a tumor suppressor in different types of human tumors [12, 23, 30, 31]. In this study, ABL2 was identified as a novel substrate to understand the molecular mechanism of FBXO31-mediated anticancer effects in TNBC. This study indicated that ABL2 protein levels were down-regulated by FBXO31 overexpression in TNBC, while increased ABL2 protein levels were observed due to the treatment with FBXO31 knockdown in TNBC cells. Furthermore, cycloheximide analysis results showed that FBXO31 overexpression obviously shortened the half-life of ABL2. It has been suggested that F-box domain of FBXO31 was required for substrate ubiquitination rather than substrate binding [10, 28]. Consistent with previous results, Co-IP results indicated that both FBXO31 and the deleted F-box of FBXO31 were capable of binding ABL2. To support this note, ubiquitination assay results revealed that only FBXO31, rather than the deleted F-box of FBXO31, enhanced ABL2 ubiquitination.

ABL kinase inhibitors have achieved great success in the treatment of chronic myeloid leukemia, prompting increasing interest in the roles of ABL1 and ABL2 in solid tumors. In contrast to the role of BCR-ABL1 in leukemia, ABL1 and ABL2 are up-regulated in solid tumors due to enhanced expression and/or activation of these kinases. ABL2 has also been suggested to promote cancer progression by enhancing cell proliferation and survival while inhibiting apoptosis. In BC, one study demonstrated that ABL2 activation promoted BC cell proliferation *in vitro*, while another report suggested that ABL2 inhibits tumor growth *in vivo.* In our study, ABL2 overexpression promotes TNBC cell proliferation, while ABL2 knockdown inhibits cell proliferation. In addition, our study found that ABL2 negatively regulated ferroptosis through down-regulating the xCT/GPX4 pathway. Furthermore, consistent with previous reports, our reports showed that ABL2 strongly promoted TNBC cell migration and invasion. Collectively, our findings indicate that ABL2 acts as an oncogenic factor in TNBC progression. However, the precise molecular mechanism by which the ABL2 kinase regulates this pathway, particularly whether it functions through direct phosphorylation of these proteins or their upstream factors, remains to be elucidated. Therefore, identifying the direct phosphorylation substrates of ABL2 in TNBC will be the central focus of our subsequent research.

To clarify whether FBXO31 exerts its tumor suppressor function through down-regulating ABL2, rescue experiments were conducted in this study. The results showed that ABL2 partly rescued the FBXO31-mediated inhibition of cell proliferation. Furthermore, ABL2 partly reversed FBXO31-mediated promotion of ferroptosis. Taken together, our study identifies ABL2 as a novel substrate of FBXO31 and elucidates a new mechanism of FBXO31-mediated cancer progression in TNBC, in which FBXO31 promotes proteasome-dependent degradation of ABL2. Thus, targeting Fbxo31 and

ABL2 may represent a potential strategy for TNBC treatment.

Conclusion

This study elucidated a novel FBXO31-ABL2-xCT/GPX4 regulatory axis in Triple-negative breast cancer (TNBC), demonstrating that FBXO31 acts as a tumor suppressor by promoting ubiquitination and degradation of ABL2, thereby enhancing ferroptosis and inhibiting malignant progression. Key findings include the following: FBXO31 is down-regulated in TNBC, and its overexpression suppresses tumor growth, migration, and invasion while inducing ferroptosis through modulation of the xCT/GPX4 pathway. ABL2 is a direct ubiquitination substrate of FBXO31. FBXO31 interacts with ABL2 via its F-box domain, leading to proteasomal degradation of ABL2 and inhibiting its oncogenic functions. In turn, ABL2 promotes TNBC progression by increasing cell proliferation and suppressing ferroptosis. Rescue experiments confirm that antitumor effects of FBXO31 are partially mediated through ABL2 down-regulation. *In vivo* validation demonstrates that FBXO31 overexpression significantly reduces tumor growth in mouse models, accompanied by reduced levels of ABL2, GPX4, and xCT. These results highlight the FBXO31-ABL2 axis as a potential therapeutic target for TNBC, offering a dual mechanism to inhibit tumor growth and sensitize cells to ferroptosis. Future studies may explore small-molecule activators of FBXO31 or ABL2 inhibitors to exploit this pathway clinically.

Acknowledgements

This work was supported by grant from Anhui Provincial Department of Education Outstanding Young Teachers Development Program in Universities (YQZD2024028), Bengbu Medical University's Incubation Project under the National Natural Science Foundation of China (2024byfy003), China National University Student Innovation & Entrepreneurship Development Program (202510367029, 202510367164), and Bengbu Medical University Graduate Student Innovation Research Project (Byycx25020).

Disclosure of conflict of interest

None.

Address correspondence to: Dr. Jia Ma, Bengbu Medical University Key Laboratory of Cancer Research and Clinical Laboratory Diagnosis, Bengbu Medical University, 2600 Donghai Avenue, Longzihu District, Bengbu 233030, Anhui, China. Tel: +86-133-0552-3667; E-mail: majiamj10@126.com; Dr. Hua Huang, Department of Biochemistry and Molecular Biology, School of Laboratory Medicine, Bengbu Medical University, 2600 Donghai Avenue, Longzihu District, Bengbu 233030, Anhui, China. Tel: +86-139-6527-1867; E-mail: huanghua@bbmu.edu.cn

References

[1] Siegel RL, Giaquinto AN and Jemal A. Cancer statistics, 2024. CA Cancer J Clin 2024; 74: 12-49.
[2] Bray F, Laversanne M, Sung H, Ferlay J, Siegel RL, Soerjomataram I and Jemal A. Global cancer statistics 2022: GLOBOCAN estimates of incidence and mortality worldwide for 36 cancers in 185 countries. CA Cancer J Clin 2024; 74: 229-263.
[3] Bianchini G, De Angelis C, Licata L and Gianni L. Treatment landscape of triple-negative breast cancer - expanded options, evolving needs. Nat Rev Clin Oncol 2022; 19: 91-113.
[4] Liu Y, Hu Y, Xue J, Li J, Yi J, Bu J, Zhang Z, Qiu P and Gu X. Advances in immunotherapy for triple-negative breast cancer. Mol Cancer 2023; 22: 145.
[5] Leon-Ferre RA and Goetz MP. Advances in systemic therapies for triple negative breast cancer. BMJ 2023; 381: e071674.
[6] Li Y, Zhang H, Merkher Y, Chen L, Liu N, Leonov S and Chen Y. Recent advances in therapeutic strategies for triple-negative breast cancer. J Hematol Oncol 2022; 15: 121.
[7] Dikic I and Schulman BA. An expanded lexicon for the ubiquitin code. Nat Rev Mol Cell Biol 2023; 24: 273-287.
[8] Tekcham DS, Chen D, Liu Y, Ling T, Zhang Y, Chen H, Wang W, Otkur W, Qi H, Xia T, Liu X, Piao HL and Liu H. F-box proteins and cancer: an update from functional and regulatory mechanism to therapeutic clinical prospects. Theranostics 2020; 10: 4150-4167.
[9] Hynes-Smith RW, Wittorf KJ and Buckley SM. Regulation of normal and malignant hematopoiesis by FBOX ubiquitin E3 ligases. Trends Immunol 2020; 41: 1128-1140.
[10] Chen K, Wang Y, Dai X, Luo J, Hu S, Zhou Z, Shi J, Pan X, Cao T, Xia J, Li Y, Wang Z and Ma J. FBXO31 is upregulated by METTL3 to promote pancreatic cancer progression via regulating SIRT2 ubiquitination and degradation. Cell Death Dis 2024; 15: 37.

[11] Liu J, Zang Y, Ma C, Wang D, Tian Z, Xu X, Li W, Jia J and Liu Z. Pseudophosphatase STYX is induced by Helicobacter pylori and promotes gastric cancer progression by inhibiting FBXO31 function. Cell Death Dis 2022; 13: 268.
[12] Duan S, Moro L, Qu R, Simoneschi D, Cho H, Jiang S, Zhao H, Chang Q, de Stanchina E, Arbini AA and Pagano M. Loss of FBXO31-mediated degradation of DUSP6 dysregulates ERK and PI3K-AKT signaling and promotes prostate tumorigenesis. Cell Rep 2021; 37: 109870.
[13] Zhu Z, Zheng Y, He H, Yang L, Yang J, Li M, Dai W and Huang H. FBXO31 sensitizes cancer stem cells-like cells to cisplatin by promoting ferroptosis and facilitating proteasomal degradation of GPX4 in cholangiocarcinoma. Liver Int 2022; 42: 2871-2888.
[14] Kumar R, Neilsen PM, Crawford J, McKirdy R, Lee J, Powell JA, Saif Z, Martin JM, Lombaerts M, Cornelisse CJ, Cleton-Jansen AM and Callen DF. FBXO31 is the chromosome 16q24.3 senescence gene, a candidate breast tumor suppressor, and a component of an SCF complex. Cancer Res 2005; 65: 11304-11313.
[15] Manne RK, Agrawal Y, Bargale A, Patel A, Paul D, Gupta NA, Rapole S, Seshadri V, Subramanyam D, Shetty P and Santra MK. A MicroRNA/ubiquitin ligase feedback loop regulates Slug-mediated invasion in breast cancer. Neoplasia 2017; 19: 483-495.
[16] Liu Y, Pan B, Qu W, Cao Y, Li J and Zhao H. Systematic analysis of the expression and prognosis relevance of FBXO family reveals the significance of FBXO1 in human breast cancer. Cancer Cell Int 2021; 21: 130.
[17] van Outersterp I, Tasian SK, Reichert CEJ, Boeree A, de Groot-Kruseman HA, Escherich G, Boer JM and den Boer ML. Tyrosine kinase inhibitor response of ABL-class acute lymphoblastic leukemia: the role of kinase type and SH3 domain. Blood 2024; 143: 2178-2189.
[18] Shang C, Huang J and Guo H. Identification of an metabolic related risk signature predicts prognosis in cervical cancer and correlates with immune infiltration. Front Cell Dev Biol 2021; 9: 677831.
[19] Zhang Z, Wang T, Xu M, Zhang Z, Wang H, Xue J and Wang W. Deciphering the pancreatic cancer microbiome in Mainland China: impact of Exiguobacterium/Bacillus ratio on tumor progression and prognostic significance. Pharmacol Res 2024; 204: 107197.
[20] Hoj JP, Mayro B and Pendergast AM. The ABL2 kinase regulates an HSF1-dependent transcriptional program required for lung adenocarcinoma brain metastasis. Proc Natl Acad Sci U S A 2020; 117: 33486-33495.
[21] Greuber EK, Smith-Pearson P, Wang J and Pendergast AM. Role of ABL family kinases in cancer: from leukaemia to solid tumours. Nat Rev Cancer 2013; 13: 559-571.
[22] Luttman JH, Colemon A, Mayro B and Pendergast AM. Role of the ABL tyrosine kinases in the epithelial-mesenchymal transition and the metastatic cascade. Cell Commun Signal 2021; 19: 59.
[23] Zhang N, Meng Y, Mao S, Ni H, Huang C, Shen L, Fu K, Lv L, Yu C, Meekrathok P, Kuang C, Chen F, Zhang Y and Yuan K. FBXO31-mediated ubiquitination of OGT maintains O-GlcNAcylation homeostasis to restrain endometrial malignancy. Nat Commun 2025; 16: 1274.
[24] Jiang X, Stockwell BR and Conrad M. Ferroptosis: mechanisms, biology and role in disease. Nat Rev Mol Cell Biol 2021; 22: 266-282.
[25] Lei G, Zhuang L and Gan B. The roles of ferroptosis in cancer: tumor suppression, tumor microenvironment, and therapeutic interventions. Cancer Cell 2024; 42: 513-534.
[26] Zhou Q, Meng Y, Li D, Yao L, Le J, Liu Y, Sun Y, Zeng F, Chen X and Deng G. Ferroptosis in cancer: from molecular mechanisms to therapeutic strategies. Signal Transduct Target Ther 2024; 9: 55.
[27] Zhang C, Liu X, Jin S, Chen Y and Guo R. Ferroptosis in cancer therapy: a novel approach to reversing drug resistance. Mol Cancer 2022; 21: 47.
[28] Johansson P, Jeffery J, Al-Ejeh F, Schulz RB, Callen DF, Kumar R and Khanna KK. SCF-FBXO31 E3 ligase targets DNA replication factor Cdt1 for proteolysis in the G2 phase of cell cycle to prevent re-replication. J Biol Chem 2014; 289: 18514-18525.
[29] Cruz Walma DA, Chen Z, Bullock AN and Yamada KM. Ubiquitin ligases: guardians of mammalian development. Nat Rev Mol Cell Biol 2022; 23: 350-367.
[30] Malonia SK, Dutta P, Santra MK and Green MR. F-box protein FBXO31 directs degradation of MDM2 to facilitate p53-mediated growth arrest following genotoxic stress. Proc Natl Acad Sci U S A 2015; 112: 8632-8637.
[31] Santra MK, Wajapeyee N and Green MR. F-box protein FBXO31 mediates cyclin D1 degradation to induce G1 arrest after DNA damage. Nature 2009; 459: 722-725.

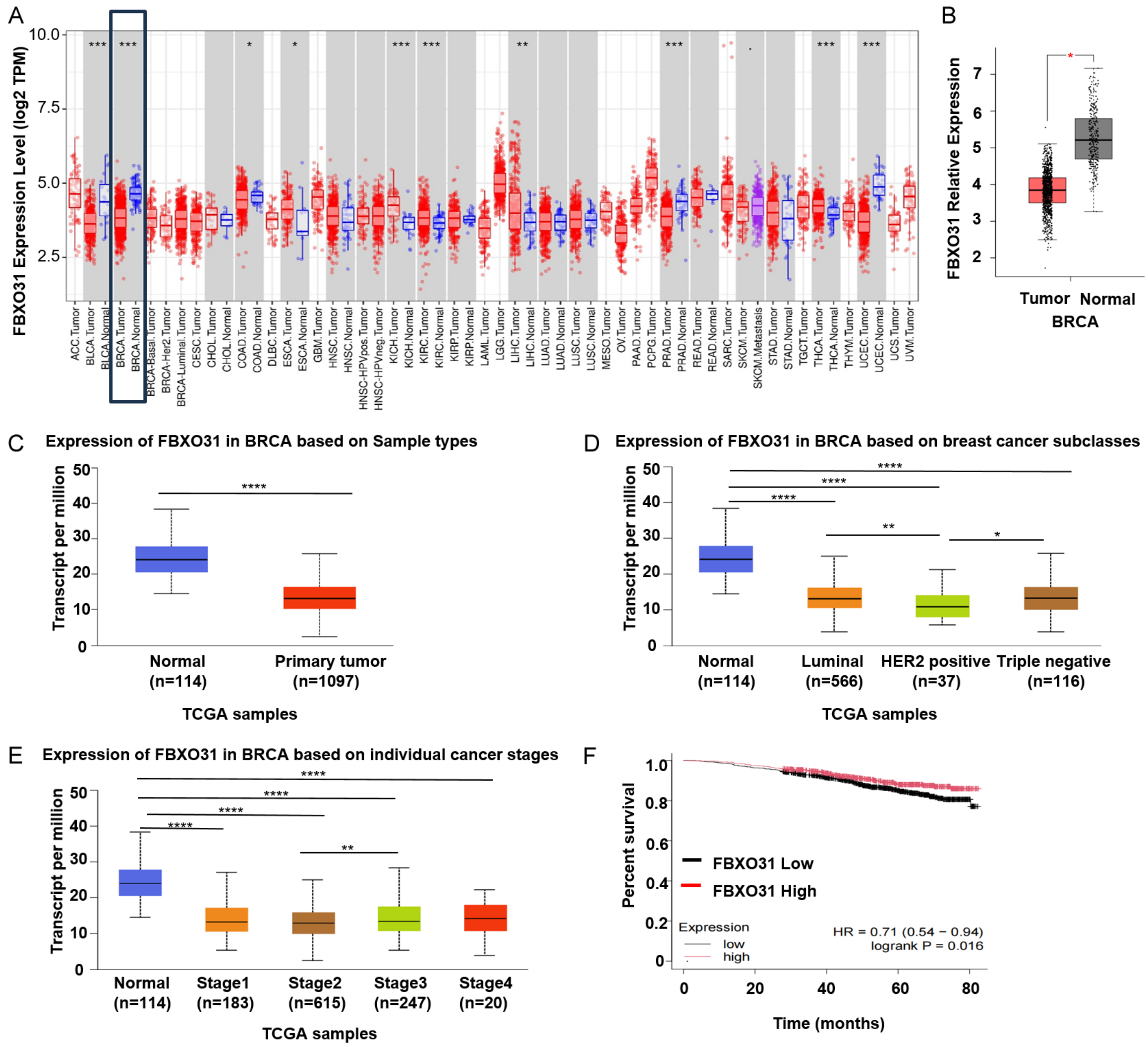

Figure S1. A. Expression levels of FBXO31 in the TCGA database in a uniform, standardized pan-cancer dataset. B. Expression levels of FBXO31 in the breast cancer dataset of the TCGA database. C. Expression of FBXO31 in BRCA based on Sample types. D. Expression of FBXO31 in BRCA based on breast cancer subclasses. E. Expression of FBXO31 in BRCA based on individual cancer stages. F. Survival curves of breast cancer patients based on FBXO31 expression. * indicates P < 0.05, ** indicates P < 0.01, *** indicates P < 0.001, **** indicates P < 0.0001.

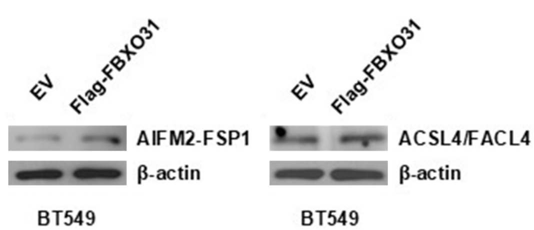

Figure S2. Western blot assays to detect the expression of Ferroptosis Suppressor Protein 1 (FSP1) and Acyl-CoA Synthetase Long-Chain Family Member 4 (ACSL4) in BT549 cells transfected with Flag-FBXO31 or empty vector (EV).

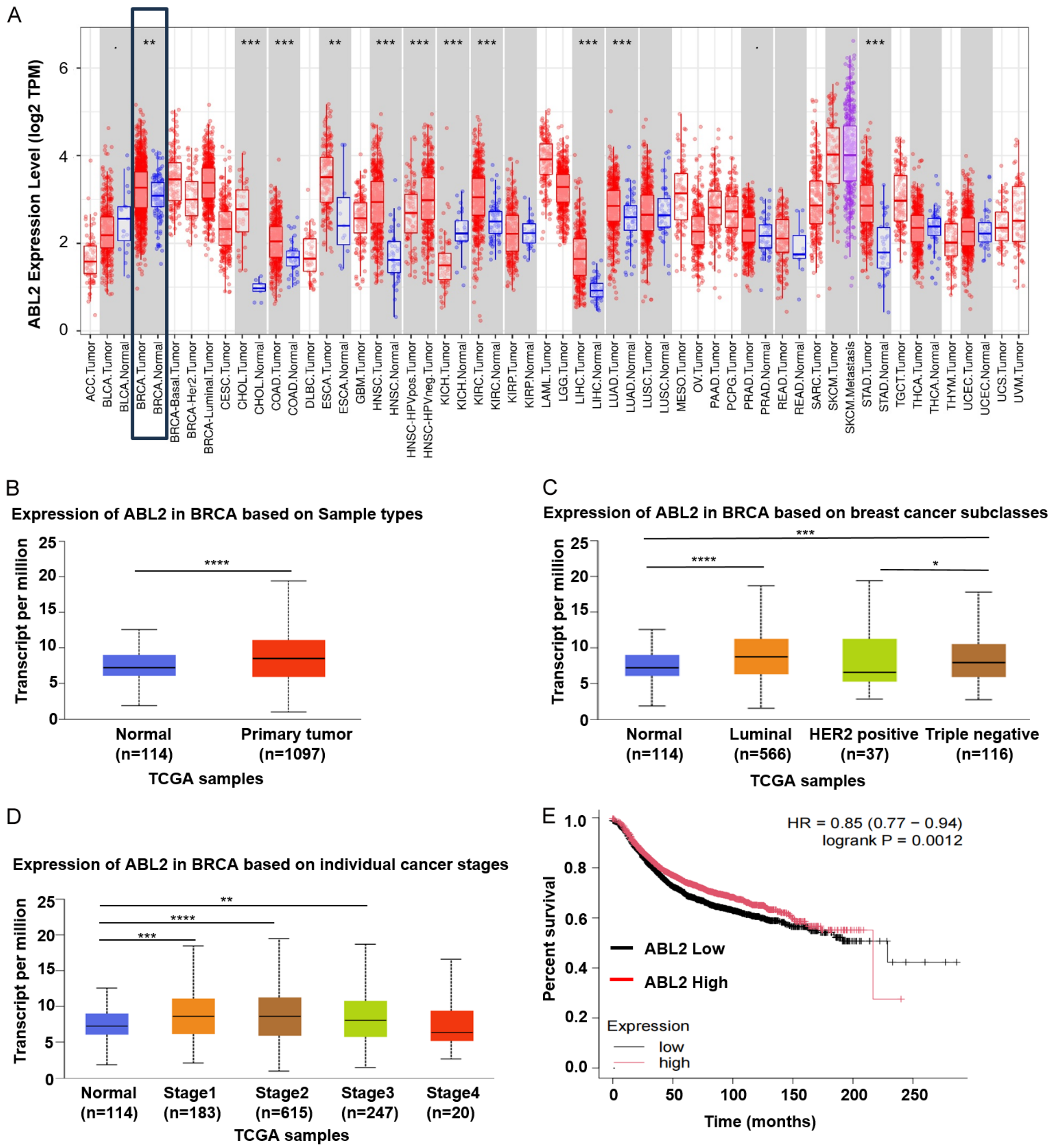

Figure S3. A. Expression levels of ABL2 in the TCGA database in a uniform, standardized pan-cancer dataset. B. Expression of ABL2 in BRCA based on Sample types. C. Expression of ABL2 in BRCA based on breast cancer subclasses. D. Expression of ABL2 in BRCA based on individual cancer stages. E. Survival curves of breast cancer patients based on ABL2 expression. * indicates P < 0.05, ** indicates P < 0.01, *** indicates P < 0.001, **** indicates P < 0.0001.

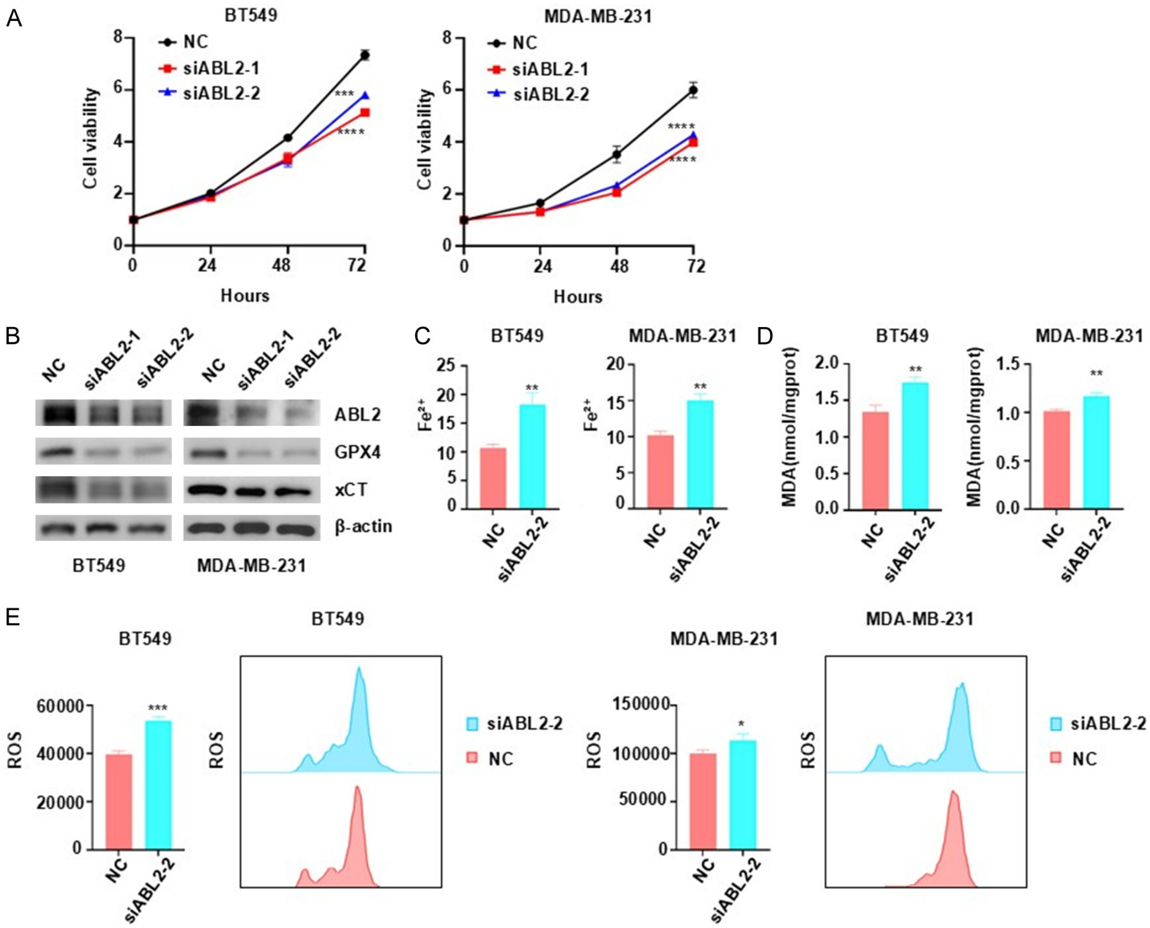

Figure S4. (A) CCK-8 assays to detect cell growth of BT549 and MDA-MB-231 cells transfected with the indicated ABL2 siRNA. (B) BT549 and MDA-MB-231 cells were transfected with ABL2 siRNA, and western blot was performed to examine changes in glutathione peroxidase 4 (GPX4) and cystine-glutamate antiporter (xCT) expression. (C-E) BT549 and MDA-MB-231 cells were transfected with ABL2 siRNA to detect cellular Fe^{2+} levels (C), MDA levels (D) and ROS levels (E). * indicates P < 0.05, ** indicates P < 0.01, *** indicates P < 0.001, **** indicates P < 0.0001.